Energy Conversion and Management: X 26 (2025) 100995

Contents lists available at ScienceDirect

Energy Conversion and Management: X

journal homepage: www.sciencedirect.com/journal/energy-conversion-and-management-x

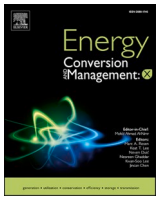

Experimental investigation of graphene-based nanofluid enhanced photovoltaic/thermal system: Energy and exergy analysis

Hussain Madhi [a,b], Sattar Aljabair [a], Ahmed Abdulnabi Imran [a], Issa Omle [c,*]

[a] Mechanical Engineering Department, University of Technology-Iraq, Baghdad, Iraq
[b] Department of Petroleum Engineering, College of Engineering, University of Misan, Misan, Iraq
[c] Institute of Physics and Electrical Engineering, University of Miskolc, Miskolc, Hungary

ARTICLE INFO

Keywords:
Exergy efficiency
Nanofluid
Fin turbulators
PV/T system
Thermal efficiency

ABSTRACT

The performance of photovoltaic (PV) modules is significantly influenced by the operating temperature, the higher temperature the lower module efficiency. The primary objective of this study is to design, fabricate, and evaluate a photovoltaic/thermal (PV/T) system equipped with a finned-serpentine channel, utilizing water and graphene nanoparticle (GnP/water) with 0.25 %, 0.5 %, 0.75 %, and 1 % concentrations as coolants at Reynold number equals to 1250. The PV/T system's performance was assessed by analyzing its energy and exergy, focusing on electrical, thermal, and exergy efficiencies. The results revealed that the PV/T system achieved electrical efficiency increments of 4.5 %, 7.6 %, 9.8 %, 13.9 %, and 15.5 % with water and NFs with 0.25 %, 0.5 %, 0.75 %, and 1 % concentrations, respectively. Furthermore, the thermal efficiency was improved by 1.4 %, 1.8 %, 2.3 %, and 2.5 % for the increased nanofluids (NFs) concentrations. The exergy efficiencies exhibited significant gains, with electrical and thermal exergy efficiencies improving by up to 15.5 % and 31.6 %, respectively, compared to water. These results highlight the substantial cooling potential of NFs to enhance the PV module's performance, which positively improves PV-related applications.

1. Introduction

Renewable energy sources, primarily solar and wind power, are considered viable alternatives to conventional energy systems because of their steady generation and potential to address gaps in energy availability [1,2]. Photovoltaic/Thermal (PV/T) systems have garnered interest for their ability to generate electrical and thermal energy concurrently. Traditional photovoltaic (PV) panels solely convert sunlight into electricity, while PV/T systems incorporate thermal cooling mechanisms, enhancing overall energy efficiency. The dual-purpose capability significantly enhances the system's performance by mitigating overheating while improving efficiency and longevity. Cooling plates on the rear surface of PV modules effectively absorb excess heat, which is then transformed into thermal energy. Additionally, implementing PV/T systems is also a substantial contribution to sustaining targets due to reducing dependence on fossil fuels and greenhouse gas emissions, which offers the possibility of cleaner energy [3,4]. Thus, PV/T systems bring economic benefits by attending to the demands of electricity and heat loads, reducing the need for separate energy systems for any residential, industrial, or commercial building. The performance of the PV/T system can be enhanced by changing the system's shape or utilising fluids with high thermophysical properties. For example, the use of finned, riffled, ribbed or structured surfaces increases the surface area for heat transmission, resulting in an improvement in the heat transfer rate [5]. Several studies have enhanced the hydrothermal performance of heat exchangers with smooth, ribbed or rifled channel designs, as well as those with straight or serpentine topologies.

Shahssavar et al. [6] conducted an empirical study on three PV/T solar collectors featuring (I) smooth, (II) three-start rifled, and (III) six-start rifled serpentine pipes. The results verified that using a six-start serpentine tube significantly enhances the energy efficiency of the PV/T system. In particular, the six-start serpentine tube exhibits a 3.8 % increase in energy efficiency (or a 22.5 % increase compared with the three-start rifled serpentine pipe) and a 1.9 % increase in exergy efficiency (or a 5.9 % increase compared with the simple serpentine pipe). Feizabadi et al. [7] conducted a numerical evaluation to examine the heat transfer rate of a twisted serpentine pipe using Al_2O_3/water NFs. The results demonstrated that straight length, serpentine pitch and twisted pitch are the primary, secondary and tertiary factors influencing the performance of the serpentine pipe. In addition, using a twisted serpentine pipe with a base fluid significantly improves hydrothermal

* Corresponding author.
E-mail address: issa.omle@uni-miskolc.hu (I. Omle).

https://doi.org/10.1016/j.ecmx.2025.100995
Received 2 February 2025; Received in revised form 12 March 2025; Accepted 28 March 2025
Available online 30 March 2025

Nomenclature

Abbreviations

PV/T	Photovoltaic thermal
PV	Photovoltaic
NF	Nanofluid
NMs	Nanomaterials
GnP	Graphene nanoparticle

Symbols

A	Area of PV panel (m^2)
C_p	Specific heat (J/kg. K)
K	Thermal conductivity (W/m. K)
D	Diameter (m)
$\dot{m}$	Mass flow rate (kg/s)
$\dot{E}x$	Exergy (w)
$\dot{E}$	Power (N/m^2)
T	Temperature (∘C)
FF	Fill factor
I	Current (A)
V	Voltage (V)
G	Solar radiation (W/m^2)
u	Speed (m/s)
H	High channel (m)
W	Width channel (m)
ΔP	Pressure drop (Pa)
Re	Reynolds number
H	Enthalpy (J/kg)
S	Entropy (J/kg. K)
$\dot{S}$	Entropy generation (J/kg. K)
Nu	Nusslt number
T	Temperature (°C)

Greek symbols

ϕ	Volume fraction (%)
ρ	Density (kg/m^3)
η	Efficiency (%)
ε	Exergy efficiency (%)
μ	Dynamic viscosity (kg/m. s)
ν	Kinematic viscosity (m^2/s)
ψ	Stream exergy per unit mass

Subscripts

B	Bulk
In	Inlet
Out	Outlet
bf	Base fluid
np	Nanoparticle
sc	Short circuit
oc	Open circuit
el	Electrical
th	Thermal
nf	Nanofluid
h	Hydraulic diameter
m	Mean
w	wind
f	fluid
amb.	Ambient
fr	Friction
gen.	Generation
tot.	Total
ov	Overall

implementation, which is 1.74–2.71 times higher than using a twisted straight pipe. This improvement can be further boosted to (3.73) times by utilising the Al_2O_3/water NFs. Bisengimana et al. [8] examined the impact of including a fin and adjusting the space between pipes in a heat exchanger within a PV/T system. The findings showed that the finned serpentine pipe with a narrow spacing achieves the most consistent temperature, resulting in a maximum efficiency of 0.984 and a minimal pressure loss of 0.073 bars. Gorzin et al. [9] performed experimental studies to examine the effect of incorporating ribs in a serpentine microchannel heat sink. The researchers analysed the distance between ribs and the number of ribs affecting the hydrothermal properties of the system. The outcomes showed that compared with the base temperatures in heat sinks without ribs using straight and serpentine channels, the base temperatures of heat sinks incorporated with ribs are reduced by 13.9 % and 7.9 %. The thermal resistance factors of the modified channel are 72 % lower than those of a simple straight channel. Furthermore, the increase in the distance of the rib decreases the temperature and the thermal resistance of the heat sink and increases the friction factor. Awais et al. [10] engaged in an experimental study to investigate how the cross-section's volumetric flow rate and length affect the pressure drop and heat transfer of a serpentine pipe heat exchanger. They studied four serpentine pipes of varying lengths: uniform length, low-to-high-to-low length, low-to-high-length, high-to-low length and high-to-low-to-high length. The investigation focused on using Al_2O_3/water NF using a concentration ranging from 1 % to 5 %. The low-to-high design demonstrates the highest heat transmission performance among the three other scenarios. Furthermore, compared with the case when the mass flow rate was 1 L/min, friction loss and heat transfer performance shows a significant increase of 95 % and 43.8 %, respectively, when the flow rate is increased to 5 L/min. Besides, compared with the serpentine pipe using only water, the serpentine pipe using an NF with a concentration of 5 % exhibits a 50 % improvement in heat transfer efficiency. Wang et al. [11] presented a numerical evaluation of the hydrothermal performance in a microchannel heat sink. They investigated the single and double microchannel configurations by considering the presence of a water/silver NF. The analysis was conducted using a two-phase model. Their findings showed that the thermal resistance of the double microchannel design is lower than that of the single design at low Re. However, both configurations exhibit similar thermal resistance as the Re increases. Additionally, the pressure drop and the heat transfer coefficient increase by 4.25 % and 12.5 %, respectively, as the nanoparticle concentration increases from 0 % to 1 %.

Recently, nanofluids (NFs) have gained significant attention due to their promising potential in improving heat transfer efficiency across a range of applications, such as solar collectors heat, exchangers, thermal energy storage, vehicle thermal systems, nuclear reactors, lubricants, detergents, and many others [12]. Compared with the traditional fluids, the NFs present improved properties like thermal conductivity, tribology, and rheological behaviour [13]. An experimental analysis has confirmed that adding nanomaterials (NMs) to the base fluids leads to significant variations in critical thermophysical properties such as dynamic viscosity and thermal conductivity [14]. Besides, NF application has been extensively explored to improve the effectiveness of heat exchange systems [15]. The recent advancement extends the scope to the radiation impact, use of green energy, sustainability, and entropy generation in magnetohydrodynamic flows [16,17,18,19,20]. These studies indicate that NFs exhibit superior heat transfer performance and highlight the significant influence of NF field conditions. This aligns with the main focus of the present research, which aims to optimize heat transfer within a boundary layer subjected to non-uniform heat sources and sinks. The main reason for choosing GnP in this research is due to the

exceptional potential of GnP in improving the thermal conductivity of formulations; thus, it is suitable for application in the cooling of PV modules. GnP with sizes ranging from 6 to 8 nm has been used to ensure its homogeneous dispersion in the base fluid, which remarkably affects enhancement in heat transfer. Four different concentrations of GnP in water were prepared, namely 0.25 %, 0.5 %, 0.75 %, and 1 %, to understand the influence of nanoparticle concentration on the thermal performance of the intended formulations. GnP were considered because of their capacity to maintain and keep constant stable thermal and rheological properties at operational temperatures between typical ranges of solar cooling systems. They are gradually attracting increasing interest because of their unique thermophysical and physicochemical properties [21]. GnP and its potential have distinct features across multiple domains- structural, optical, thermal, electronic, and mechanical properties, making it highly applicable for various applications [22,23]. Besides, GnP is universally available at competitive prices. The high surface area, outstanding conductivity, and easy functionalization of GnP make it an optimal substrate for synthesising metallic GnP varieties [24].

Many studies have been conducted to analyze the very high impacts of the thermophysical properties of these NFs on the performance of PV/T systems. For example, Venkatesh et al. [25] proved that applying a mixture of GnP/water, having a concentration of 0.3 vol%, reduced the temperature of the PV/T system by 60 °C to 45 °C, corresponding to an increment of about 13 % in electrical efficiency. In a study with a similar approach, Alshikhi and Kayfeci [26] analyzed the impacts of aluminium oxide (Al_2O_3) and GnP NFs on the operation of PV/T systems at a flow rate of 0.5 l/min, and both were used at a 0.5 wt% concentration, concerning water. Their results showed that energy efficiency was significantly improved with GnP/H_2O, which improved efficiency by up to 56.1 %. In another work, Alwan Sywan Alshaheen et al. [27] discovered that GnP/H_2O NFs at a concentration of 0.05 wt% and a flow rate of 50 kg/h produced total energy efficiency of 19.3 %, exceeding the effect of SWCNT/H_2O as well as MWCNT/H_2O NFs. Another analysis was performed by Taheri et al. [28] using deionized water, GnP/H_2O, SWCNT/H_2O, MWCNT/H_2O NFs, maintaining their concentration at 0.05 wt%, and a flow rate of 50 kg/h. The highest increase in exergy efficiency, 2.32 %, was for GnP/H_2O NFs. The studies collectively demonstrate that GnP/water significantly improves the efficiency of PV/T systems and promises the achievement and even exceeding of expected performance enhancements. The NFs extremely high thermal conductivity and heat transfer properties are necessary to increase the thermal, electrical, and overall efficiency of PV/T systems.

1.1. Novelty

This study experimentally investigates the effects of four different concentrations of NFs on both the electrical and thermal efficiencies of a PV/T system. The selected NFs consist of GnP dispersed in water, and the experiments are conducted under a constant mass flow rate. An uncertainty analysis is performed on the experimental data to ensure the results' reliability. The primary focus of this research is to assess the actual performance of a PV/T system incorporating finned serpentine channels in addition to the NFs effect from an exergy perspective. While numerous studies have investigated PV/T systems, research on entropy generation in such systems remains limited in the literature. Therefore, this study aims to assess the thermal, electrical, and exergy efficiencies of a PV/T system enhanced with a finned serpentine channel and NFs at varying concentrations offering valuable insights for further advancements in renewable energy technologies.

1.2. Motivation

GnP is considered among the most advanced two-dimensional materials available today. These NMs have gained significant attention due to their outstanding physicochemical and thermophysical properties. GnP presents outstanding characteristics in the structural, optical, thermal, electronic, and mechanical aspects and thus can be applied over a wide range. Besides, it is very easy to acquire at very competitive pricing, and thus, it comes very well recommended. Its exceptional properties, such as high surface area, exceptional conductivity, and ease of functionalization, make it one of the best constituents of metallic GnP nanocomposites.

1.3. Application

Nanotechnology is vital in addressing energy exchange challenges across various fields, including solar energy, chemical engineering, semiconductors, space exploration, bioengineering, electronics, and biosensors. Researchers continually seek to enhance these processes through advanced methodologies and innovative techniques. This study aims to improve heat transfer efficiency by employing NFs, which consist of nanoparticles uniformly dispersed within a base fluid. Research findings indicate that NFs exhibit superior heat retention capabilities compared to conventional fluids, making them highly beneficial in various applications, such as transportation, industrial processes, nuclear safety, and thermal management in electronic devices. Additionally, NFs enhance thermal performance in both industrial and technological systems while improving efficiency in the mechanical components of aircraft and automobiles.

2. Experimental work

2.1. System setup and equipment

The experiment was conducted on the rooftop of the Misan University's College of Engineering in Iraq (47.14°N, 31.84°E). The PV/T systems were set at a 30° tilt facing south and operated between 8:00 AM and 5:00 PM, as shown in Fig. 1. Two poly-crystalline PV modules were used, each rated at 50 W with dimensions of 66 mm × 56 mm × 3 mm. The specifications for the PV/T system are listed in the table. One module served as a reference, while the other was modified with a plate and fins placed at a 30° angle, a configuration shown in earlier studies to yield optimal performance [29]. The fins were attached with thermal adhesive to ensure proper thermal conductivity. The entire setup was housed in a serpentine channel to generate turbulence, which enhances heat transfer. The collector was mounted on the back of the PV module using thermal glue and secured with clamps, ensuring a strong attachment. A helical copper spiral was positioned inside a water tank, with one port connected to the PV/T system's outlet and the other linked to an NFs reservoir to facilitate heat dissipation see Fig. 2. The collector was insulated with thermal wool and aluminium to minimize energy loss. More details for design specifications and characteristics of the PV/T system are shown in Table 1.

In this study, GnP/water was used as the cooling medium and data was collected using a multichannel Arduino AT mega 2560, supplied by Ardunic Sinaa in Baghdad. This device was equipped with current and voltage sensors to measure output current and voltage and K-type thermocouples to monitor temperatures. The fluid circulation was regulated by a pump positioned within the NF tank. The working fluid maintained a constant mass flow rate of 44 kg/h in all experiments. A sensor of flow was installed between the pump and the inlet to monitor and measure the flow rate continuously. A thermocouple was used to track the ambient temperature. Solar radiation levels were recorded every 30 min using a solar power meter. Signal Express 2015 software-managed data acquisition and retrieval, ensuring systematic data collection at 30-minute intervals. The specifications of the measurement devices are provided in Table 2. Sudden fluctuations in weather, mainly changes in solar radiation due to cloud cover and variations in ambient temperature, can influence the performance of the PV/T system. The experiments were conducted during August and September to obtain more consistent results with reduced uncertainty when weather

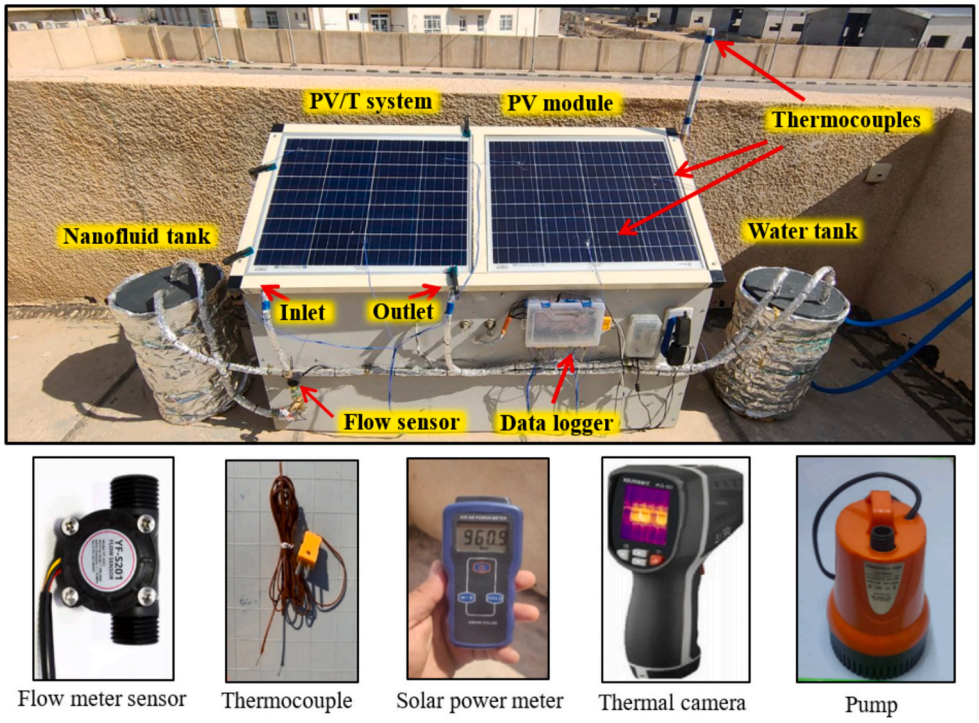

Fig. 1. Experimental setup and measurement instrumentation.

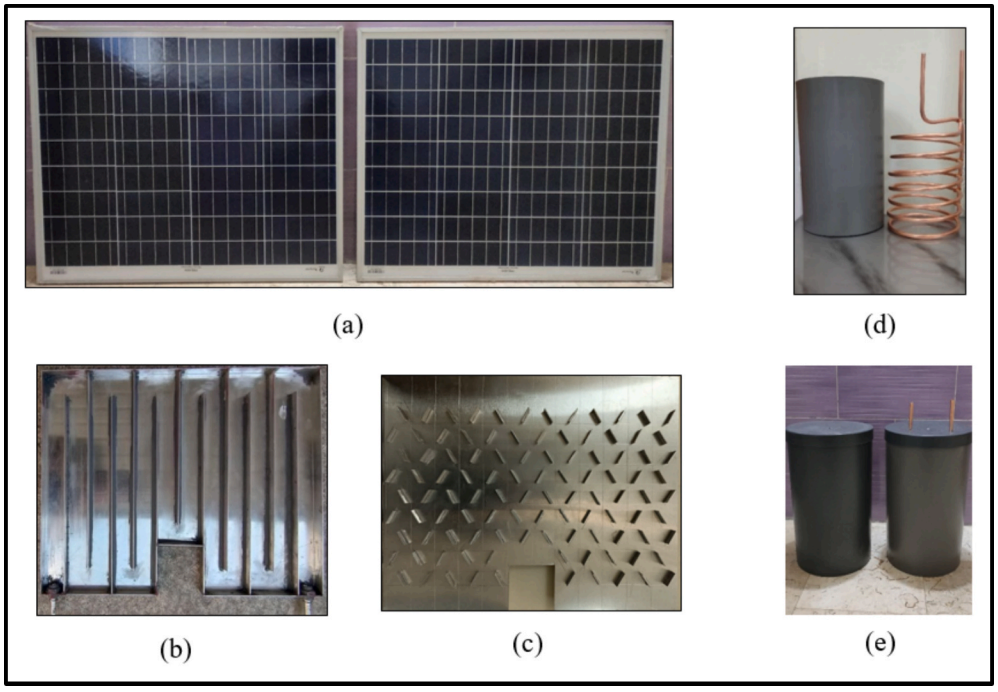

Fig. 2. Experimental parts of PV/T systems: (a) PV panels, (b) collector with serpentine channels, (c) fins with 30°, (d) helical coil and (e) water and NFs tanks.

conditions, ambient temperature, and solar irradiation remained relatively stable.

2.2. Preparation of NFs

Preparing NFs aims to enhance the thermophysical properties of base fluids by improving thermal conductivity. The two-step process is widely utilised among the various methods for synthesizing NFs. This process typically involves either a single-step approach, such as chemical or physical vapour deposition, or a two-step technique where NMs are dispersed into a base fluid. The efficiency of nanoparticle dispersion plays a crucial role in minimizing sedimentation rates and ensuring the long-term stability of the NFs. These factors are heavily dependent on the preparation method. By incorporating nanoparticles into the base fluid, the resulting NFs exhibit significantly enhanced thermophysical properties, leading to improved heat transfer performance. In this study, high-purity GnP with a particle size of 20 nm were sourced from Skyspring NMs, Inc. (Houston, TX, USA). Four

Table 1
Design specifications and characteristics of the PV/T system.

PV solar cell (at standard testing conditions)	
Poly-crystalline	Type
50	Maximum power (W)
650 × 550	PV Dimension (mm)
3	Glass thickness (mm)
36	Number of cells
16	Cell efficiency (%)
22.28	Open-circuit voltage (v)
2.88	Short-circuit current (A)
Collector design	
Finned-serpentine channel	Type
Aluminium	Materials
2	Thickness(mm)
12	Number of channels
108	Number of fins
30 × 20	Area of fins (mm)
600 × 480	Area of collector (mm)
430 × 25	Area of baffles (mm)
40	Insulation thickness (mm)

Table 2
Details of sensor and measurement device specifications.

Item	Range	Model	Accuracy	Units
Pump	1000	LH-1600C	–	L/h
Flow rate sensor	1–30	YF-S201	±9%	L/min
Thermocouples	−200 to 1350	K (3 m length)	0.25	°C
Voltage sensor	up to 25	Module 25 V	0.02445	V
Solar power meter	1–3999	SM209	10	W/m^2
Current sensor	up to 30	ACS712	0.04	A
Ultrasonic bath	240:40	040S	–	W/kHz
Electronic scale	3	BOECO BAS	0.0001 g	kg

concentrations of GnP/water were prepared, namely (0.25-1) vol.%, by dispersing the nanoparticles in water. The quantities of nanoparticles were carefully measured using an electronic scale, then dispersed in water and mixed for 25 min using a magnetic stirrer. An ultrasonic bath with a 10 L capacity was utilized for 35 min to prevent particle agglomeration and ensure a uniform suspension, as illustrated in Fig. 3. The stability of the prepared NFs was evaluated by sedimentation and visualization techniques at intervals of 2 and 10 h after ultrasonic treatment, as shown in Fig. 4. The results indicate that the NFs have sufficient stability, confirming the practicality of producing the required quantities for subsequent experimental studies. The uniform dispersion of nanoparticles in the base fluid is important for preventing sedimentation and improving the stability and overall performance of the NFs. The key factor affecting the suspension and stability of nanoparticles is

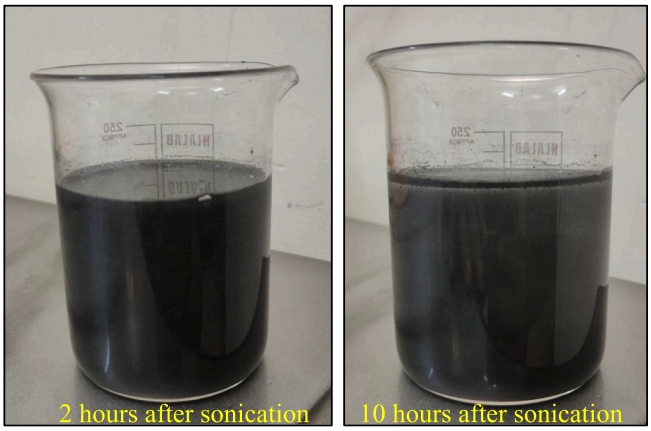

Fig. 4. Stability of GnP/water NFs at different periods.

Brownian motion, which plays an important role in maintaining the uniform distribution of nanoparticles in the liquid [30,31]. This phenomenon describes the random movement of nanoparticles due to collisions with liquid molecules. As a result, the NFs exhibit long-term stability and high thermal efficiency, making them suitable for a wide range of heat transfer applications. The integration of nanoparticles and the influence of Brownian motion play a vital role in improving the heat transfer performance of nanofibers, thereby enhancing their overall effectiveness in thermal management systems.

The characteristics of the GnP utilized in this study are summarized in Table 3. Notably, the thermal conductivity of these nanoparticles is significantly higher than water's. The NF properties were evaluated using the thermal characteristics of GnP/water and applying the equation (1) which used to estimate the density of the NFs [32].

$$\rho_{nf} = (1-\phi)\rho_{bf} + \phi\rho_{np} \quad (1)$$

Where (ϕ) is a volumetric concentration of the NFs, which was determined by the following equation [33]:

Table 3
Thermophysical properties of GnP/water.

Substance	K (W/m·K)	ρ (kg/m^3)	C_p (J/kg.K)	μ (kg/m.s)	Thickness (nm)	Purity
Water	0.613	997.1	4179	0.001	–	–
GnP	3000	3600	710	–	6–8	99.5 %

Fig. 3. Ultrasonic cleaner and magnetic stirrer of GnP/water.

$$\phi = \frac{\dot{m}_{np}\rho_{np}}{\dot{m}_{np}\rho_{np} + \dot{m}_{bf}\rho_{bf}} \tag{2}$$

Equation (3) was employed to evaluate the specific heat of NFs [18].

$$\rho C_{pnf} = \rho C_{pnp}\phi + (1-\phi)\rho C_{pbf} \tag{3}$$

The dynamic viscosity of NFs was determined using the following equation [34]:

$$\mu_{nf} = \frac{\mu_{bf}}{(1-\phi_{np})^{2.5}} \tag{4}$$

The thermal conductivity of NFs was evaluated using the model presented below [35]:

$$k_{nf} = \frac{(k_{np} + 2k_{bf} + 2\phi(k_{np} - k_{bf}))k_{bf}}{k_{np} + 2k_{bf} - \phi(k_{np} - k_{bf})} \tag{5}$$

2.3. Data reduction

In studying finned-serpentine channels and PV/T systems, a thorough understanding of the governing equations is crucial for accurately analysing heat transfer and fluid dynamics. The Reynolds number (Re) is a key dimensionless parameter that characterizes the flow regime within the channel. It is defined as: [36]

$$Re = \frac{u_m \times D_h}{\nu} \tag{6}$$

Where u_m denotes the average velocity, and ν is the kinematic viscosity, D_h refers to the hydraulic diameter, which can be determined from the following equation [37]:

$$D_h = \frac{2(W \times H)}{W + H} \tag{7}$$

This equation considers the channel's geometry, where H and W represent the height and width, respectively.

The heat transfer coefficient between the surrounding environment and the glass layer was calculated using the following method by using wind velocity as $u_w = 1.5$ m/s [38]:

$$h_w = 5.7 + (3.8 \times u_w) \tag{8}$$

Nu is a crucial parameter that links convective heat transfer to conductive heat transfer. It is given by the following expression [39,40]:

$$Nu = \frac{h \times D_h}{k}, \tag{9}$$

The thermal conductivity of the fluid is represented by k, while h stands for the heat transfer coefficient.

The electrical efficiency η_{el} of the PV/T system is determined by the following expression [41]:

$$\eta_{el} = \frac{V \times I \times FF}{G \times A} \tag{10}$$

The power output, denoted as $\dot{E}_{el}$, is calculated using equation (11). Here, V represents the voltage, I stands for the current, G is the solar intensity, and A refers to the area of the PV/T surface. The fill factor FF measures the maximum PV efficiency and can be determined using the following equation (12) [36].

$$\dot{E}_{el} = V \times I \tag{11}$$

$$FF = \frac{V_{pv} \times I_{pv}}{V_{oc} \times I_{sc}} \tag{12}$$

The thermal efficiency η_{th} is calculated using the following equation [42]:

$$\eta_{th} = \frac{\dot{m}C_p \times (T_{out} - T_{in})}{G \times A} \tag{13}$$

In this equation, C_p represents the specific heat capacity, $\dot{m}$ denotes the mass flow rate, and T_{out} and T_{in} refer to the outlet and inlet temperatures, respectively.

The exergy analysis follows a similar approach to the energy analysis method. The exergy balance equation is expressed as follows, considering the PV module and collector design under steady-state conditions [43]:

$$\sum \dot{E}x_{in} = \sum \dot{E}x_{out} + \sum \dot{E}x_{loss} \tag{14}$$

$$\dot{E}x_{sun} + \dot{E}x_{mass,in} = \dot{E}x_{el} + \dot{E}x_{mass,out} + \dot{E}x_{loss} \tag{15}$$

In this equation, $\dot{E}x$ represents the exergy rates with $\dot{E}x_{loss}$, $\dot{E}x_{out}$, and $\dot{E}x_{in}$ corresponding to the exergy rates for losses, output, and input, respectively. The solar exergy rate, $\dot{E}x_{sun}$ is calculated based on the solar radiation incident on the system [44].

$$\dot{E}x_{sun} = G\left(1 - \frac{T_{amb.}}{T_{sun}}\right) \tag{16}$$

$T_{amb.}$ represents the ambient temperature, while T_{sun} denotes the sun's temperature, which is assumed to be 5800 K. The exergy associated with the mass flow rate is expressed as [45]:

$$\dot{E}x_{mass,out} - \dot{E}x_{mass,in} = \dot{m}_f(\psi_{out} - \psi_{in}) \tag{17}$$

where

$$\psi_{out} = (h_{out} - h_{amb.}) - T_{amb.}(s_{out} - s_{amb.}) \tag{18}$$

$$\psi_{in} = (h_{in} - h_{amb.}) - T_{amb.}(s_{in} - s_{amb.}) \tag{19}$$

In this equations, s and h represent the entropy and enthalpy values, respectively. Since electrical energy is regarded as a form of available helpful energy, the electrical power generated by the PV module is considered equivalent to its exergy [46].

$$\dot{E}x_{el} = \dot{E}_{el} \tag{20}$$

Equations (18) and (19) are substituted into equation (15), yielding the following expression [43]:

$$G\left(1 - \frac{T_{amb.}}{T_{sun}}\right) - \dot{E}x_{el} - \dot{m}_f[(h_{out} - h_{in}) - T_{amb.}(s_{out} - s_{in})] = \dot{E}x_{loss} \tag{21}$$

The changes in enthalpy and entropy of the flow are defined as [44]:

$$\Delta h = (h_{out} - h_{in}) = C_{p,nf}(T_{out,nf} - T_{in,nf}) \tag{22}$$

$$\Delta s = (s_{out} - s_{in}) = C_{p,nf}\ln\left(\frac{T_{out,nf}}{T_{in,nf}}\right) \tag{23}$$

In equation (21), the term $\dot{E}x_{loss}$ represents only the exergy losses associated with heat transfer. Therefore, it will be referred to as $\dot{E}x_{loss,Q}$ in subsequent formulations. Furthermore, another source of exergy loss, stemming from fluid friction within the collector, is discussed as follows [47]:

$$\dot{E}x_{loss,fr} = \frac{\dot{m}_{nf}\Delta P}{\rho_f}\frac{T_{amb.}ln(\frac{T_{out,nf}}{T_{in,nf}})}{T_{out,nf} - T_{in,nf}} \tag{24}$$

Where ΔP represents the pressure drop across the collector, the entropy generation is calculated as follows [45]:

$$\dot{S}_{gen,tot} = \frac{\dot{E}x_{loss,tot}}{T_{amb.}} = \frac{\dot{E}x_{loss,Q} + \dot{E}x_{loss,fr}}{T_{amb.}} = \dot{S}_{gen,Q} + \dot{S}_{gen,fr} \quad (25)$$

$\dot{S}_{gen,tot}$ refers to the total entropy generation, while $\dot{S}_{gen,Q}$ represents the entropy generation caused by heat transfer. On the other hand, $\dot{S}_{gen,fr}$ is the entropy generation due to fluid friction. The total exergy efficiency of the PV/T system is defined as a combination of thermal and electrical exergy efficiencies [46].

$$\varepsilon_{ov} = \frac{\dot{E}x_{th} + \dot{E}x_{el}}{\dot{E}x_{sun}} \quad (26)$$

In Equations (27) and (28), efficiencies of electrical and thermal exergy are expressed as follows [43]:

$$\varepsilon_{el} = \frac{\dot{E}x_{el}}{\dot{E}x_{sun}} = \frac{\dot{E}_{el}}{G\left(1 - \frac{T_{amb.}}{T_{sun}}\right)} = \frac{V_{oc} \times I_{sc} \times FF}{G\left(1 - \frac{T_{amb.}}{T_{sun}}\right)} \quad (27)$$

$$\varepsilon_{th} = \frac{\dot{E}x_{th}}{\dot{E}x_{sun}} = \frac{\dot{m}_{nf} \times C_{p,nf} \times [(T_{out,nf} - T_{in,nf}) - T_{amb.} ln(\frac{T_{out,nf}}{T_{in,nf}})]}{G\left(1 - \frac{T_{amb.}}{T_{sun}}\right)} \quad (28)$$

2.4. Uncertainty analysis

An uncertainty analysis was performed for the instruments used in the experimental setup, as well as for the relevant physical quantities, in order to determine the measurement errors. The uncertainties associated with physical quantities such as thermal efficiency, electrical efficiency, and power output are expressed in Equations (29), (30), and (31). These uncertainties were calculated using standard methodologies [48,49]. A summary of the uncertainty assessment is provided in Table 4.

$$\frac{UP}{P} = \sqrt{\left(\frac{UV}{V}\right)^2 + \left(\frac{UI}{I}\right)^2} \quad (29)$$

$$\frac{U\eta_{el}}{\eta_{el}} = \sqrt{\left(\frac{UV}{V}\right)^2 + \left(\frac{UI}{I}\right)^2 + \left(\frac{UG}{G}\right)^2 + \left(\frac{UFF}{FF}\right)^2} \quad (30)$$

$$\frac{U\eta_{th}}{\eta_{th}} = \sqrt{\left(\frac{UG}{G}\right)^2 + \left(\frac{U\dot{m}}{\dot{m}}\right)^2 + \left(\frac{UT}{T}\right)^2} \quad (31)$$

2.5. Estimation of PV/T economic feasibility

A key aspect of this study involves evaluating the proposed cooling technique's economic implications compared to conventional PV modules. This assessment is essential for determining the payback period of PV/T systems. The analysis considers various factors, including minimal maintenance requirements, operational costs related to components such as the pump and flow sensor, and overall energy consumption. The hybrid PV/T system consists of multiple components, including an aluminium finned-serpentine channel, cover, pump, insulation, plastic tubing, and plastic containers. The net profit is calculated using equation (32) [50], a specific formula that integrates the costs associated with each component. Compared to standard PV modules, the hybrid PV/T systems, which incorporate finned-serpentine channels and NFs, exhibit a payback period of 746 days. In contrast, conventional PV modules show a longer payback period of 835 days. Additional details are shown in Table 5. This discrepancy supports the hypothesis that integrating NFs improves the economic viability and efficiency of the PV/T systems.

Net profit = energy production costs (electrical and thermal) − cost of NFs − operational costs − maintenance expenses (32)

Table 4
Measurement uncertainty.

No.	Parameter	Symbols	Values	Range of uncertainty %
1	Power	P	15.71–41.38	0.76–0.8
2	Electrical efficiency	η_{el}	9.96–15.8	0.21–0.88
3	Thermal efficiency	η_{th}	34.81–50.51	4.7–6.78

3. Results and discussion

Weather data in Al Amarah has been compared with regional and global trends to provide a broader understanding of climate patterns. Al Amarah, located in a semi-arid climate, experiences rising temperatures consistent with warming trends across the Middle East. Its precipitation patterns fluctuate similarly to those in neighboring regions, such as western Iran, Kuwait, Saudi Arabia, and the UAE, where the hot desert climate is characterized by extremely high temperatures and dry summers, with cooler winters and occasional rainfall [51]. Given these similarities, specific findings from the study can be generalized to regions with comparable climatic conditions. This comparative analysis underscores the interconnected nature of climate dynamics, reinforcing the credibility of the study's conclusions while providing a foundation for climate adaptation strategies in Al Amarah and similar environments. Fig. 5 illustrates the average daily weather data collected in Al Amarah City at the University of Misan. The highest recorded ambient temperature was 48 °C, and the highest solar radiation reached 1160 W/m^2. The data show temperature and solar radiation fluctuations, with the peak values occurring at 12:30 PM, followed by a steady decrease towards the end of the observation period.

The placement of thermocouples on both the front and rear sides of the system illustrates the impact of cooling on the PV temperature throughout the experiment, especially when compared to the reference PV module. The reference PV module reached a high temperature of 70 °C due to the increased surface temperature caused by direct exposure to sunlight. The cooling effect using NFs enhances heat exchange by utilizing finned-serpentine channels (cooler than the back of the PV panel) and the rear side, typically the hottest part. This process improves the heat transfer rate between the circulating NFs and the conductive channels, reducing the PV/T system temperature. The thermophysical properties of the nanoparticles suspended in the water further promote convective heat transfer between the collector and the GnP/water NFs. As a result, compared to the PV module, the surface temperature of the PV/T system showed a significant reduction at 12:30 PM. This temperature drop is attributed to water and NFs (GnP/water) circulation at concentrations of 0.25 %, 0.5 %, 0.75 %, and 1 %. The average temperature reductions increase by 13.3 %, 16.6 %, 17.5 %, 18.4 %, and 19.2 % were observed, as shown in Fig. 6. These findings highlight the effectiveness of GnP/water NFs as suitable working fluid, attributed to their superior thermophysical properties and the high purity of the nanoparticles. Additionally, implementing finned-serpentine channel designs is crucial in enhancing heat transfer. These techniques induce vortices and promote turbulent flow, effectively disrupting the thermal boundary layer that forms on the upper surface of the collector. As a

Table 5
Estimation of PV/T economic feasibility using NFs.

Components/Aspects	PV module	PV/T system
Configurations	35 $	172 $
Maintenance	0.00397 $/day	0.007 $/ day
Operation cost	–	0.00367 $/ day
NF supply	–	0.056 $/day
Energy productivity	0.0459 $/day	0.297 $/day
Net profit	0.0419 $/day	0.230 $/day
Payback period	835 days	746 days

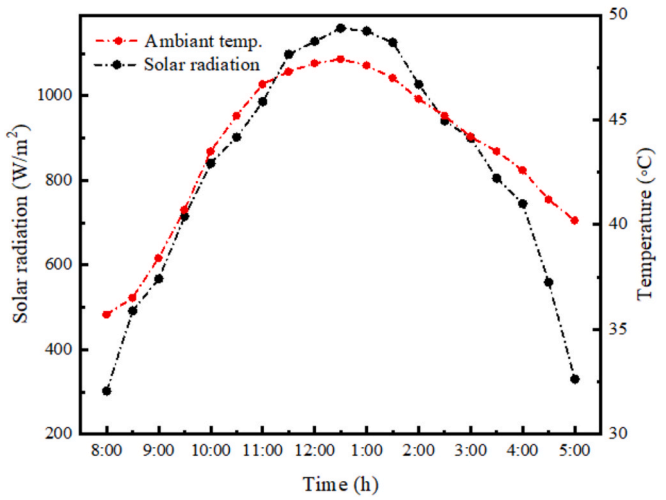

Fig. 5. Solar radiation intensity and atmospheric temperatures.

result, the heat transfers between the PV module and the NFs are significantly improved, leading to a substantial enhancement in the overall performance and efficiency of the system [29].

Fig. 7 highlights the improvement in electrical power generated by the PV/T systems using GnP/water NFs at concentrations of 0.25 %, 0.5 %, 0.75 %, and 0.1 %. The data demonstrate the significant cooling potential of these NFs at all concentrations. This enhancement is attributed to the role of NMs in facilitating improved heat exchange between the back of the PV modules and the collector. The mechanisms behind this include enhanced heat transfer through both convection and conduction, which ultimately lowers the PV/T system's temperature compared to the uncooled configuration. The electrical power output of the reference PV module was lower due to a reduction in the open-circuit voltage, which was influenced by increasing temperature. When the system was cooled with water, 0.25 %, 0.5 %, 0.75 %, and 0.1 % NFs, the average electrical power increased by 4.6 %, 7.8 %, 10.2 %, 14.4 and 15.8 %, respectively. This increase in electrical power can be attributed to the higher open-circuit voltage resulting from the combined effect of the thermophysical properties of NFs and the optimized finned-serpentine channel design. The decrease in temperature contributed to higher electrical output in the PV/T system. The enhanced thermal performance is due to the efficient heat transfer between the hot surface of the PV modules and the cooler absorbing plate, leading to the overall improvement in PV/T system operation [52].

Reducing the temperature of the PV module led to increased power output, thereby improving both the thermal and electrical efficiencies. High temperatures adversely affected the performance of the PV panel, causing the electrical efficiency of the reference PV module to drop to 8.8 %. However, circulating water, 0.25 %, 0.5 %, 0.75 %, and 0.1 % through the collector resulted in a temperature reduction and enhanced the average electrical efficiency by 4.4 %, 7.5 %, 9.8 %, 13.8 %, and 15.5 %, respectively see Fig. 8 (a). The circulation of these NFs effectively lowered the temperature at the rear of the PV/T systems, thereby boosting both power and electrical efficiency. The data demonstrate that using GnP/water NFs significantly improved thermal efficiency compared to water cooling alone, which achieved an average value of only 21.17 %. The introduction of NFs improved thermal efficiency by 1.4 %, 1.8 %, 2.3 %, and 2.5 %, respectively, at concentrations of 0.25 %, 0.5 %, 0.75 %, and 0.1 % NFs, as shown in Fig. 8 (b). The results demonstrate that integrating GnP/water into the PV/T system enhances their performance by improving electrical and thermal conductivity. Furthermore, integrating the finned serpentine channels improves heat transfer from the PV surface to the collector. This design helps to reduce cell temperature and improves thermal stability, which is critical for maintaining long-term efficiency. These advances can significantly contribute to developing more efficient solar systems suitable for various industrial applications. Potential uses include large-scale solar thermal power plants, where improved heat dissipation can increase system reliability and performance. In addition, improved thermal management in PV/T hybrid systems is also beneficial, as it can generate electricity and heat simultaneously. This is particularly beneficial for agricultural applications such as industrial heating, desalination plants, and greenhouse heating. In addition, these findings can support the development of efficient solar panels for space applications, where thermal regulation is a key challenge.

The second law of thermodynamics plays a vital role in assessing the efficiency of energy systems by evaluating the energy output and the quality of energy conversion. An exergy analysis was performed to evaluate the performance of the PV/T system. Fig. 9 (a) illustrates the variation in the electrical exergy efficiency of the PV/T system using GnP/water NFs. The results show that incorporating a collector into the PV module significantly improves electrical exergy efficiency. However, as the system approaches solar noon, the increase in electrical exergy slows down relative to the increase in solar radiation. This is primarily due to the high temperatures of the PV module, which reduces its efficiency. Consequently, the electrical exergy efficiency increased by 4.5 %, 7.6 %, 9.8 %, 13.9 %, and 15.5 % using water, 0.25 %, 0.5 %, 0.75 %, and 0.1 % NFs, respectively.

Fig. 9(b) further investigates the effect of the working fluid on the thermal efficiency of the PV/T system. The thermal energy efficiency is still relatively low due to the low quality of the generated thermal energy. However, NFs significantly improve the system performance compared to water due to their better thermal conductivity and more efficient heat transfer between the collector and the coolant. When the NF concentration is 0.25 %, 0.5 %, 0.75 % and 0.1 %, the thermal efficiency is improved by 18.6 %, 19.3 %, 23.9 % and 31.6 %, respectively. The results of this study hold significant implications for practical applications across various industrial and engineering fields. The GnP's improved thermal conductivity can enhance solar water heaters' efficiency by optimizing heat absorption and transfer in domestic hot water systems. Moreover, this NFs can be applied in drying systems, where effective heat exchange is critical for reducing energy consumption and increasing drying rates. In solar cooling systems, the enhanced heat dissipation properties of the NFs can contribute to better temperature regulation, thereby improving the overall performance and lifespan of PV modules. These applications underscore the potential of GnP/water NFs as advanced heat transfer fluids, supporting the development of more sustainable and energy-efficient thermal management solutions.

Analyzing entropy generation in thermodynamic systems is crucial for identifying energy losses. In PV/T systems, evaluating entropy generation and exergy loss provides valuable insights into their overall performance. Fig. 10(a) illustrates the daily exergy loss due to heat transfer in a PV/T system using water and different concentrations of NFs. The results show that the PV module and the PV/T system experience significant exergy losses, primarily due to their low efficiency. Given the system's low thermal exergy efficiency, the exergy losses in the PV module and the PV/T system are nearly identical. The total entropy generation in a PV/T system originates mainly from heat transfer and, to a lesser extent, from fluid friction within the collector. As shown in Fig. 10(b), the daily variation in entropy generation due to heat transfer increases as the system approaches solar noon, increase the heat exchange between the PV/T system and its surroundings. Additionally, over time, the aggregation of nanoparticles in the NFs can lead to increased system irreversibility, contributing further to entropy generation. To reduce these effects, it is important to implement an effective cooling mechanism in PV/T systems, which can help reduce exergy loss. Using NFs improves heat transfer and reduces this exergy loss compared to conventional cooling fluids. Since the mass flow rate and temperature difference between the collector's inlet and outlet are relatively small, the exergy loss caused by fluid friction is minimal. On average, the exergy loss due to fluid friction across all working fluids is around 2.25

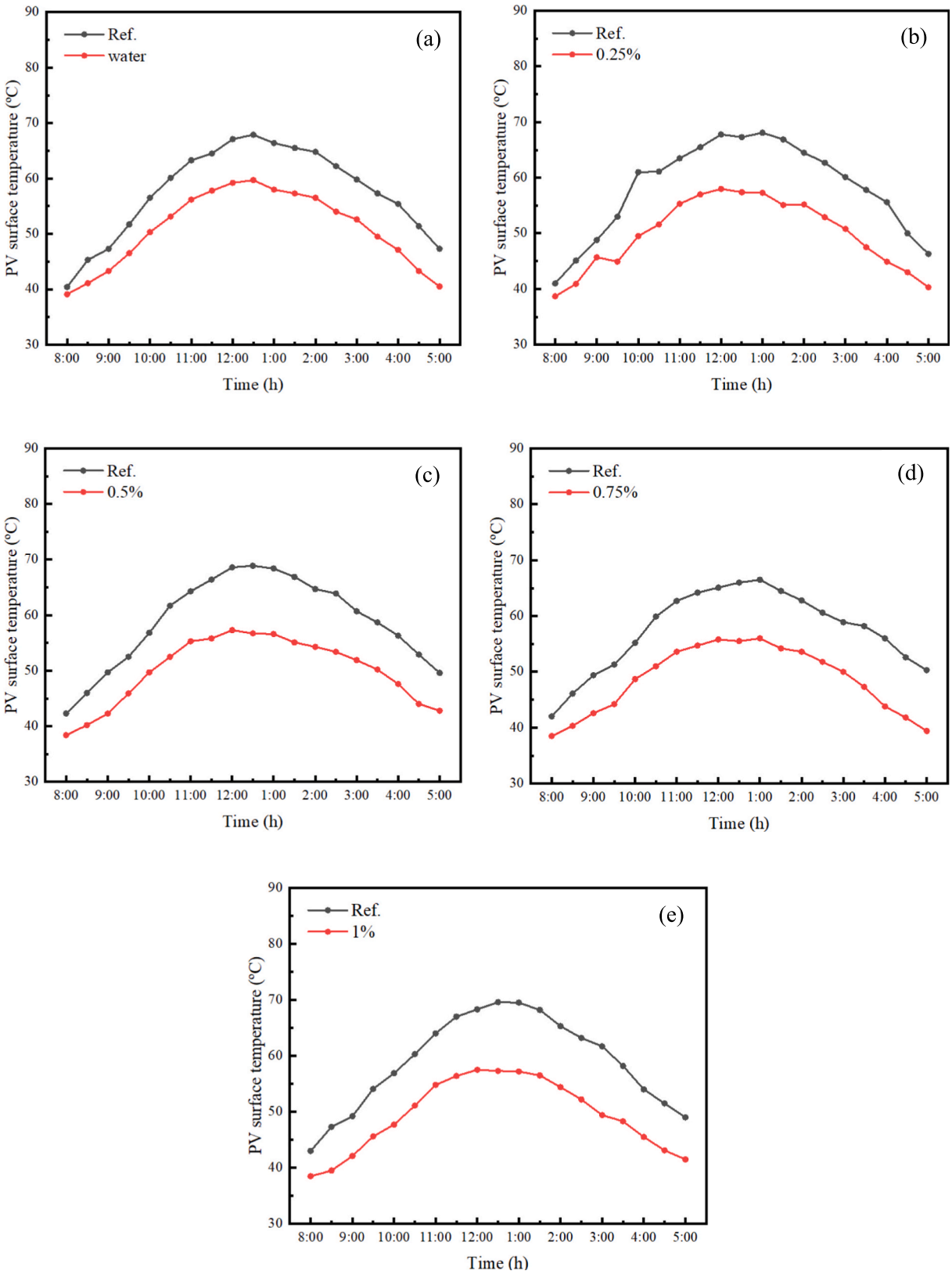

Fig. 6. The surface temperature of PV/T systems compared with reference utilizing NFs concentration at (a) water, (b) 0.25%, (c) 0.5%, (d) 0.75%, and (e) 1%.

W/m^2 per day, which makes its impact on entropy generation small compared to heat transfer. Among the fluids tested, the PV/T system with NFs shows the lowest exergy loss and entropy generation, while the water-based system shows the highest values. Water has lower thermal and electrical exergy, leading to higher losses and more significant entropy generation. The reduction in entropy generation in the PV/T system is 0.92 %, 1.2 %, 1.6 %, 2.1 %, and 2.3 % for water and NFs with concentrations of 0.25 %, 0.5 %, 0.75 %, and 1 %, respectively. As entropy generation increases, the system becomes more irreversible, leading to higher exergy losses and decreased efficiency. Reducing

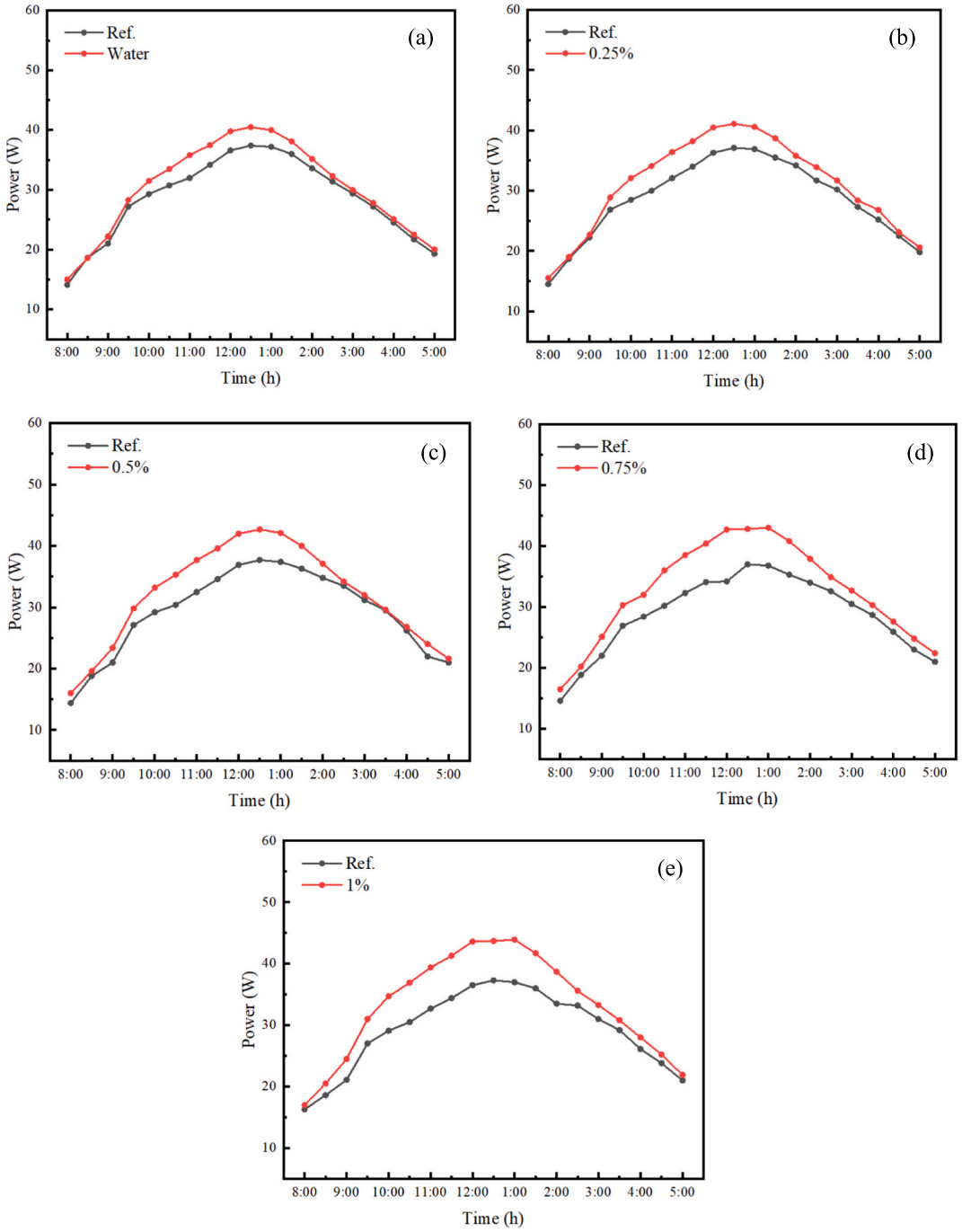

Fig. 7. Electrical power generated by the PV/T systems utilizing NFs concentration at water, (b) 0.25%, (c) 0.5%, (d) 0.75%, and (e) 1%.

entropy generation helps maintain higher exergy levels, reduce waste, and improve the system's overall performance. This shows that minimizing entropy generation is crucial for enhancing the efficiency of PV/T systems.

Table 6 illustrates the effect of nanoparticle concentration on pressure drop (ΔP), pump power consumption, total electrical output, and net electrical output of the PV/T system. The relationship between nanoparticle concentration and energy consumption can be observed by analysing the data, where increasing the nanoparticle concentration affects system performance through several interconnected factors. It is noted that increasing the nanoparticle concentration leads to a rise in pressure drop within the system, which directly impacts pump power consumption. For example, when transitioning from water to a 0.25 % concentration, the pressure drop increased from 1170 Pa to 1177 Pa, resulting in a rise in pump power consumption from 11.04 W.h/day to 11.48 W.h/day. In contrast, the net electrical output increased from 261.21 W.h/day to 266.17 W.h/day, indicating a positive performance gain that outweighed the increase in pump power consumption. This trend continues at a 0.5 % concentration, with pump power consumption rising to 12.76 W.h/day, while the net electrical output increased to 273.06 W.h/day. The difference between the gain in net electrical output and the increase in pump power consumption remains positive, suggesting that the benefits of adding nanoparticles are still effective. However, at higher concentrations, such as 0.75 % and 1 %, a sharp rise in pump power consumption is observed, reaching 14.04 W.h/day and 16.60 W.h/day, respectively. Although total electrical output continues to increase, the difference between the gain in electrical power and the pump power consumption starts to shrink, indicating that the system is

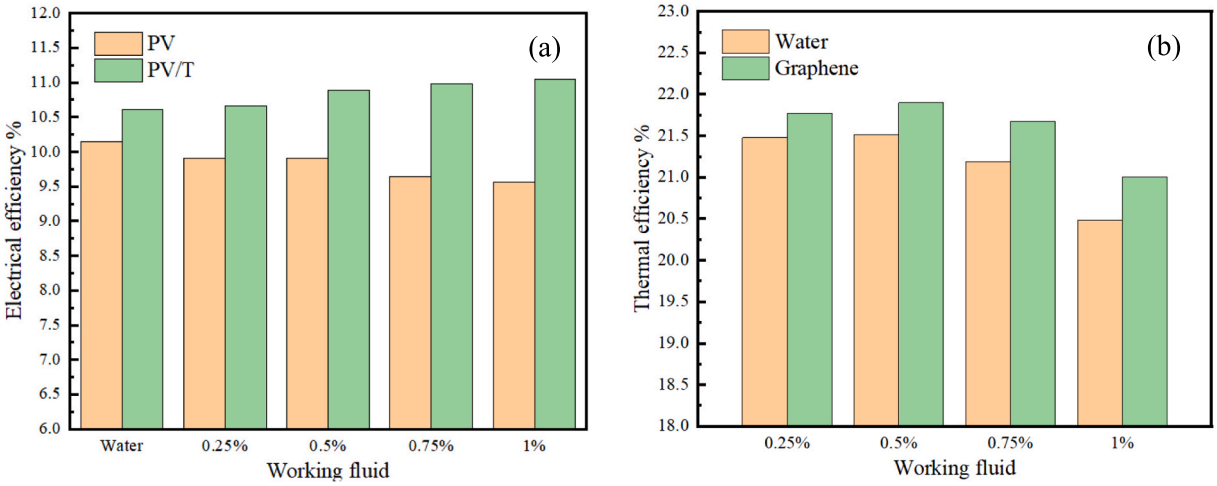

Fig. 8. (a) Electrical and (b) thermal efficiencies of PV/T systems utilizing variable NF concentrations.

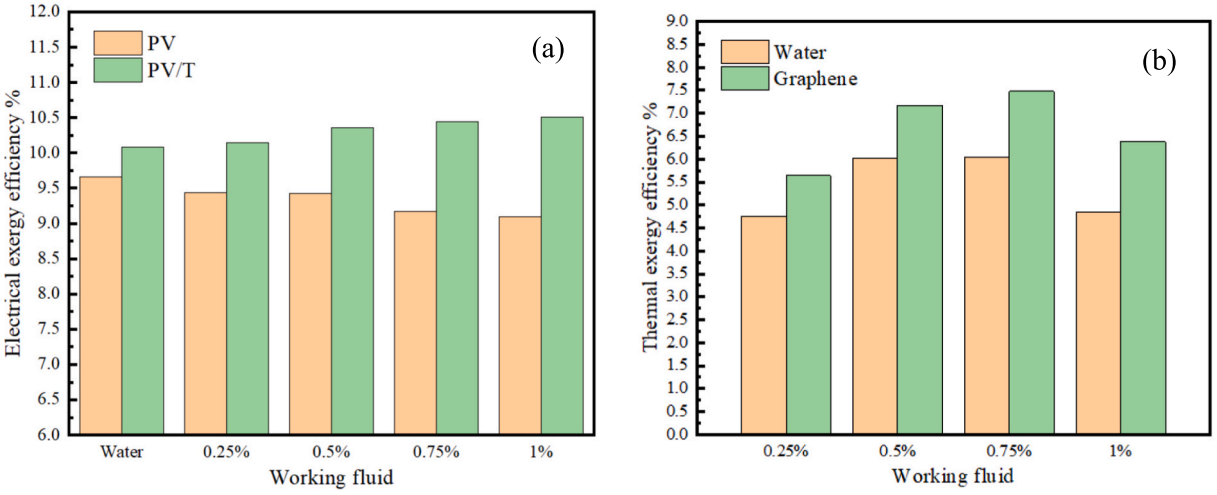

Fig. 9. Average exergy efficiencies for the (a) thermal and (b) electrical outputs of the PV unit and the PV/T system.

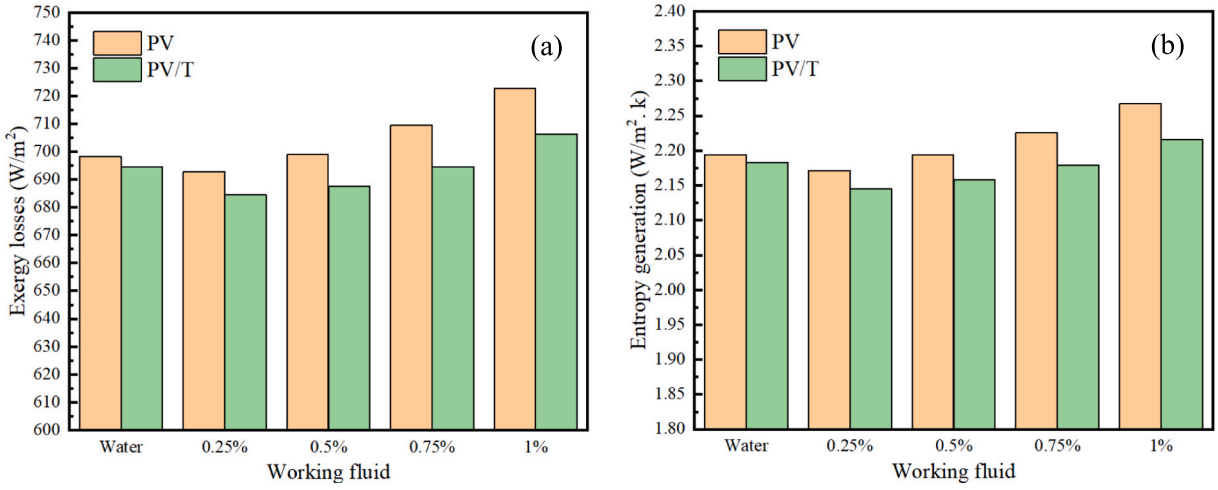

Fig. 10. (a) Daily exergy losses and (b) variation of entropy generation in the PV/T system.

approaching a saturation point where the negative effects of increased pump consumption become more significant. Based on these findings, it can be concluded that increasing nanoparticle concentration enhances the PV/T system's electrical performance, but this improvement remains effective only up to a specific limit. Beyond this threshold, the increased density of the NFs negatively impacts system efficiency due to the

Table 6
Net electrical output data for the PV/T system with a flow rate of 44 kg/h.

Volume concentration	Pressure drop (ΔP) (pa)	Consumed Pump Power (W. h/day)	PV/T Electrical (W. h/ day)	PV/T Net electrical output (W. h/ day)
water	1170	11.04	272.25	261.21
0.25 %	1177	11.48	277.65	266.17
0.5 %	1185	12.76	285.82	273.06
0.75 %	1196	14.04	294.39	280.35
1 %	1209	16.60	300.51	283.91

substantial rise in pump power consumption. Therefore, selecting an optimal concentration that maximizes electrical output while minimizing additional energy losses is recommended to ensure the highest operational efficiency of the system.

Table 7 compares the efficiency parameters for the PV/T system in this study with those reported in previous research. Although the system does not outperform every other configuration in terms of individual electrical or thermal efficiency, the overall energy yield is significantly higher compared to the other systems. For example, while the Serpentine tube collector achieves a higher electrical efficiency of 17.33 % and others exhibit higher thermal efficiencies (e.g., Header-riser collector at 54.7 %), the fin-serpentine channels configuration demonstrates a more balanced and optimized performance. It achieves 15.44 % electrical efficiency and 45.6 % thermal efficiency, which might seem lower compared to specific individual configurations. However, these two values result in a much higher total energy output when combined. The key reason for this improvement lies in the combined performance of electrical and thermal outputs in the finned-serpentine channels. By improving heat transfer through enhanced turbulence, the finned-serpentine channels ensure that thermal and electrical efficiencies contribute effectively to the overall energy production.

4. Technology limitations and insights for future work

Although the current study has shown notable outcomes in terms of PV/T system energy efficiency, as well as the exergy and economic aspects, it still has some limitations. The exceptional weather conditions of the location under study present a major challenge. Therefore, the results of this work are expected to be slightly different under other weather conditions. Besides, the PV/T scale influences the results since the PV module size directly influences its efficiency.

For new incomers to this research field, the following insights could be highlighted in this work to develop and optimize the study further:

- It is important to explore new types of nanoparticles, focusing on cost-effectiveness, stability, and the ability to maintain the required concentration levels.
- The design of the heat exchanger could be optimized by incorporating other fin types with different materials to explore the cooling potential and its effect on the PV/T performance.
- New technologies that combine NFs with phase change materials (PCMs) and fins hold great promise. These need to be carefully investigated, considering both system complexity and economic considerations.
- The economic viability of using NFs in large-scale PV/T systems is still a challenging task in this work due to cost concerns. Therefore, assessing the feasibility of large NF quantities and considering both initial and operating costs are necessary.
- Future investigations could explore the impact of different fin materials, as well as variations in fin width and length, to assess their effects at different mass flow rates. Furthermore, studies could examine the optimal number of channels to determine the most efficient design that minimizes heat loss and reduces manufacturing costs.
- Although visual sedimentation analysis was used to evaluate the stability of NFs, it is recommended that additional analytical tests, such as Zeta Potential measurements, be conducted to verify the long-term stability of NFs.
- A detailed Exergy Analysis could be conducted to study the irreversibilities, identify sources of energy loss, and develop strategies to minimize these losses, improving overall system performance and efficiency.

Table 7
PV/T thermal and electrical efficiencies are based on previous studies considering various collector configurations.

Collector configuration	Flow direction	Electrical efficiency (%)	Thermal efficiency (%)	Reference
Header–riser collector, PV/T system	Parallel flow	7.20	54.7	[53]
Serpentine collector, PV/T system	Serpentine flow	7.46	57.1	[53]
Serpentine tube collector, PV/T system	Serpentine flow	17.33	26.87	[54]
Straight channel collector, PV/T system	Straight flow	12.9	47.2	[55]
Helical channel collector, PV/T system	Straight flow	13.5	57.9	[55]
Bionic channel collector, PV/T system	Straight flow	14.5	33.5	[56]
Serial channel collector, PV/T system	Serial flow	14.3	–	[56]
Parallel channel collector, PV/T system	Straight flow	14.4	–	[56]
Fin turbulator	Serpentine flow	15.44	45.6	Present study

5. Conclusion

This study aims to improve the performance of a photovoltaic/thermal (PV/T) system by developing an advanced cooling unit that combines fins with serpentine channels and nanofluids (NFs) for uniform cooling. The energy and exergy efficiency of the system are evaluated at different solar irradiance levels and different NF concentrations. An integrated approach combining experimental analysis with thermodynamic evaluations is used to quantify the impact of these modifications. The results show that electrical and thermal efficiencies significantly improve when using NFs compared to conventional water-based cooling systems. Specifically, the electrical efficiency increases to 4.4 %, 7.5 %, 9.8 %, 13.8 %, and 15.5 % when the NF concentrations are 0.25 %, 0.5 %, 0.75 %, and 1 %, respectively. The thermal efficiency increases by 1.4 %, 1.8 %, 2.3 %, and 2.5 % at the same NF concentrations. In addition, the thermal energy efficiency is also significantly improved, increasing by 18.6 %, 19.3 %, 23.9 %, and 31.6 %, respectively. Notably, integrating NFs reduces the exergy losses and entropy generation by 2.2 % and 2.3 %, respectively, compared to the water-based system. The results of this study highlight the effectiveness of modern cooling techniques in optimizing the performance of PV/T systems, making a significant contribution to the field. Integrating fins with serpentine channels and NFs represents an innovative approach to improve heat dissipation, minimize energy losses, and increase the sustainability of solar energy applications. These results provide valuable insights for future research and development of more efficient hybrid PV/T systems.

CRediT authorship contribution statement

Hussain Madhi: Writing – original draft, Visualization, Resources, Investigation. **Sattar Aljabair:** Writing – review & editing, Supervision, Methodology. **Ahmed Abdulnabi Imran:** Writing – review & editing, Supervision, Formal analysis, Data curation. **Issa Omle:** Writing – review & editing, Visualization, Validation, Funding acquisition, Supervision.

Funding

The research was funded by the EKÖP-24-4-I, supported by the University Research Scholarship Program of the Ministry for Culture and Innovation through the National Research, Development, and Innovation Fund.

Declaration of competing interest

The authors declare that they have no known competing financial interests or personal relationships that could have appeared to influence the work reported in this paper.

Data availability

Data will be made available on request.

References

[1] Najim N, Hussany F, Flayh S. Design of water pumping mechanism using wind energy (analysis study). Misan J Eng Sci 2022;1(2):95–111. https://doi.org/10.61263/mjes.v1i2.35.
[2] Mohammed Radhi S, Al-Majidi S, Abbod M, Al-Raweshidy H. Predicting solar power generation utilized in iraq power grid using neural network. Misan J Eng Sci 2024;3(1):38–62. https://doi.org/10.61263/mjes.v3i1.72.
[3] Alktranee M, Al-Yasiri Q, Saeed Mohammed K, Al-Lami H, Bencs P. Energy and exergy assessment of a photovoltaic-thermal (PVT) system cooled by single and hybrid nanofluids. Energy Convers Manag X 2024;24:100769. https://doi.org/10.1016/j.ecmx.2024.100769.
[4] Eriksen AB, Kosinski P, Balakin BV, Kosinska A. Experimental study of a direct absorption solar collector with stationary nanofluid. Energy Convers Manag X 2024;23:100683. https://doi.org/10.1016/j.ecmx.2024.100683.
[5] Zhang G, Huang H, Sun T, Zhang Z. Flow structures and heat transfer on small-scale concentric ribs rough surface for confined turbulent jet impingement. Int Commun Heat Mass Transf 2022;137:106218. https://doi.org/10.1016/j.icheatmasstransfer.2022.106218.
[6] Shahsavar A, Shahmohammadi M, Askari IB. CFD simulation of the impact of tip clearance on the hydrothermal performance and entropy generation of a water-cooled pin-fin heat sink. Int Commun Heat Mass Transf 2021;126:105400. https://doi.org/10.1016/j.icheatmasstransfer.2021.105400.
[7] Feizabadi A, Khoshvaght-Aliabadi M, Rahimi AB. Numerical investigation on Al2O3/water nanofluid flow through twisted-serpentine tube with empirical validation. Appl Therm Eng 2018;137:296–309. https://doi.org/10.1016/j.applthermaleng.2018.03.076.
[8] Bisengimana E, Zhou J, Binama M, Yuan Y. Numerical investigation on the factors influencing the temperature distribution of photovoltaic/thermal (PVT) evaporator/condenser for heat pump systems. Renew Energy 2022;194:885–901. https://doi.org/10.1016/j.renene.2022.05.154.
[9] Gorzin M, Ranjbar AA, Hosseini MJ. Experimental study on serpentine minichannel heat sink: Effect of rib existence and distance. Int J Therm Sci 2022;173:107397. https://doi.org/10.1016/j.ijthermalsci.2021.107397.
[10] Awais M, Saad M, Ayaz H, Ehsan MM, Bhuiyan AA. Computational assessment of Nano-particulate (Al2O3/Water) utilization for enhancement of heat transfer with varying straight section lengths in a serpentine tube heat exchanger. Therm Sci Eng Prog 2020;20:100521. https://doi.org/10.1016/j.tsep.2020.100521.
[11] Wang D, et al. A comparative numerical analysis and environment assessment to examine hydrothermal behavior of two serpentine heatsink with water/silver Nano fluid applying two-phase mixture model. Eng Anal Bound Elem 2023;146:966–76. https://doi.org/10.1016/j.enganabound.2022.09.010.
[12] Shang Y, et al. Artificial neural network hyperparameters optimization for predicting the thermal conductivity of MXene/graphene nanofluids. J Taiwan Inst Chem Eng 2024;164:105673. https://doi.org/10.1016/j.jtice:2024.105673.
[13] Sepehrnia M, Maleki H, Forouzandeh Behbahani M. Tribological and rheological properties of novel MoO3-GO-MWCNTs/5W30 ternary hybrid nanolubricant: Experimental measurement, development of practical correlation, and artificial intelligence modeling. Powder Technol 2023;421:118389. https://doi.org/10.1016/j.powtec.2023.118389.
[14] Jasim DJ, et al. Enhancing solar energy conversion efficiency: thermophysical property predicting of MXene/graphene hybrid nanofluids via Bayesian-optimized artificial neural networks. Results Eng 2024;24:102858. https://doi.org/10.1016/j.rineng.2024.102858.
[15] Vinoth R, Sachuthananthan B, Vadivel A, Balakrishnan S, Raj AGS. Heat transfer enhancement in oblique finned curved microchannel using hybrid nanofluid. Int J Therm Sci 2023;183:107848. https://doi.org/10.1016/j.ijthermalsci.2022.107848.
[16] Nasir S, Berrouk AS, Aamir A. Efficiency analysis of solar radiation on chemical radioactive nanofluid flow over a porous surface with magnetic field. Case Stud Therm Eng 2024;63:105231. https://doi.org/10.1016/j.csite.2024.105231.
[17] Nasir S, Berrouk A, Aamir A. Exploring nanoparticle dynamics in binary chemical reactions within magnetized porous media: a computational analysis. Sci Rep 2024;14(1):25505. https://doi.org/10.1038/s41598-024-76757-4.
[18] Saleem Nasir ASB, Gul T. Analysis of chemical reactive nanofluid flow on stretching surface using numerical soft computing approach for thermal enhancement. Eng Appl Comput Fluid Mech 2024;18(1):2340609. https://doi.org/10.1080/19942060.2024.2340609.
[19] Nasir S, Sirisubtawee S, Juntharee P, Berrouk AS, Mukhtar S, Gul T. Heat transport study of ternary hybrid nanofluid flow under magnetic dipole together with nonlinear thermal radiation. Appl Nanosci 2022;12(9):2777–88. https://doi.org/10.1007/s13204-022-02583-7.
[20] Nasir S, Berrouk AS. Comparative study of computational frameworks for magnetite and carbon nanotube-based nanofluids in enclosure. J Therm Anal Calorim 2024;149(5):2403–23. https://doi.org/10.1007/s10973-023-12811-z.
[21] Dey A, Ahmed ZU, Alam MR. Thermal and exergy analysis of pin-finned heatsinks for nanofluid-cooled high-concentrated photovoltaic thermal (HCPV/T) hybrid systems. Energy Convers Manag X 2022;16:100324. https://doi.org/10.1016/j.ecmx.2022.100324.
[22] Abbas S, Nisa ZU, Nazar M, Amjad M, Ali H, Jan AZ. Application of heat and mass transfer to convective flow of Casson fluids in a microchannel with Caputo–Fabrizio derivative approach. Arab J Sci Eng 2024;49(1):1275–86. https://doi.org/10.1007/s13369-023-08351-1.
[23] Ali N. Graphene-based nanofluids: production parameter effects on thermophysical properties and dispersion stability. Nanomater Basel 2022;12(3):357. https://doi.org/10.3390/nano12030357.
[24] Borode AO, Ahmed NA, Olubambi PA, Sharifpur M, Meyer JP. Investigation of the thermal conductivity, viscosity, and thermal performance of graphene nanoplatelet-alumina hybrid nanofluid in a differentially heated cavity. Front Energy Res 2021;9(August):1–15. https://doi.org/10.3389/fenrg.2021.737915.
[25] Venkatesh T, Manikandan S, Selvam C, Harish S. Performance enhancement of hybrid solar PV/T system with graphene based nanofluids. Int Commun Heat Mass Transf 2022;130:105794. https://doi.org/10.1016/j.icheatmasstransfer.2021.105794.
[26] Alshikhi O, Kayfeci M. Experimental investigation of using graphene nanoplatelets and hybrid nanofluid as coolant in photovoltaic thermal systems. Therm Sci 2022;26(1):195–208. https://doi.org/10.2298/TSCI200524348A.
[27] Alshaheen AAS, Kianifar A, Rahimi AB. Experimental study of using nano-(GNP, MWCNT, and SWCNT)/water to investigate the performance of a PVT module. J Therm Anal Calorim 2020;139(6):3549–61. https://doi.org/10.1007/s10973-019-08724-5.
[28] Taheri A, Kazemi M, Amini M, Sardarabadi M, Kianifar A. The performance assessment of nanofluid-based PVTs with and without transparent glass cover: outdoor experimental study with thermodynamics analysis. J Therm Anal Calorim 2021;143(6):4025–37. https://doi.org/10.1007/s10973-020-09311-9.
[29] Madhi H, Aljabair S, Imran AA. Comparative numerical study on the effect of fin orientation on the photovoltaic/thermal (PV/T) system performance. Int J Thermofluids 2024;24(October):100909. https://doi.org/10.1016/j.ijft.2024.100909.
[30] Habib S, Nasir S, Khan Z, Berrouk AS, Waseem Islam S. Machine learning-driven analysis of heat transfer in chemically reactive fluid flow considering Soret-Dufour effects. Int J Thermofluids 2025;25:100982. https://doi.org/10.1016/j.ijft.2024.100982.
[31] Nasir S, et al. Three-dimensional rotating flow of MHD single wall carbon nanotubes over a stretching sheet in presence of thermal radiation. Appl Nanosci 2018;8(6):1361–78. https://doi.org/10.1007/s13204-018-0766-0.
[32] Madhi H, Aljabair S, Imran AA. A review of photovoltaic/thermal system cooled using mono and hybrid nanofluids. Int J Thermofluids 2024;22:100679. https://doi.org/10.1016/j.ijft.2024.100679.
[33] Alktranee M, Al-Yasiri Q, Shehab MA, Bencs P, Németh Z, Hernadi K. Experimental and numerical study of a photovoltaic/thermal system cooled by metal oxide nanofluids. Alexandria Eng J 2024;94:55–67. https://doi.org/10.1016/j.aej.2024.03.050.
[34] Habeeb AS, Aljabair S, Karamallah AA. Experimental and numerical assessment on hydrothermal behaviour of MgO-Fe3O4/H2O hybrid nano-fluid. Int J Thermofluids 2022;16:100231. https://doi.org/10.1016/j.ijft.2022.100231.
[35] Habeeb AS, Aljabair S. Computational Single and Multiphase Approaches to Investigate the Hydrothermal Behavior of Hybrid Nano-fluid in Plain and Wavy Tubes 2023;41, no. October 2022:886–903.
[36] Yazdanifard F, Ameri M, Ebrahimnia-Bajestan E. Performance of nanofluid-based photovoltaic/thermal systems: A review. Renew Sustain Energy Rev 2017;76:323–52. https://doi.org/10.1016/j.rser.2017.03.025.
[37] Imran AA, Mahmoud NS, Jaffal HM. Analysis of channel configuration effects on heat transfer enhancement in streamline-shaped cold plates used in battery cooling system: A comparative study. Int Commun Heat Mass Transf 2024;155:107570. https://doi.org/10.1016/j.icheatmasstransfer.2024.107570.

[38] Sardarabadi M, Passandideh-Fard M. Experimental and numerical study of metal-oxides/water nanofluids as coolant in photovoltaic thermal systems (PVT). Sol Energy Mater Sol Cells 2016;157:533–42. https://doi.org/10.1016/j.solmat.2016.07.008.
[39] Jaffal HM, Mahmoud NS, Imran AA, Hasan A. Performance enhancement of a novel serpentine channel cooled plate used for cooling of Li-ion battery module. Int J Therm Sci 2023;184:107955. https://doi.org/10.1016/j.ijthermalsci.2022.107955.
[40] Hamza NFA, Aljabair S. Evaluation of thermal performance factor by hybrid nanofluid and twisted tape inserts in heat exchanger. Heliyon 2022;8(12):Dec. https://doi.org/10.1016/j.heliyon.2022.e11950.
[41] Hosseinzadeh M, Sardarabadi M, Passandideh-Fard M. Energy and exergy analysis of nanofluid based photovoltaic thermal system integrated with phase change material. Energy 2018;147:636–47. https://doi.org/10.1016/j.energy.2018.01.073.
[42] Imran AA, Mahmoud NS, Jaffal HM. Numerical and experimental investigation of heat transfer in liquid cooling serpentine mini-channel heat sink with different new configuration models. Therm Sci Eng Prog 2018;6:128–39. https://doi.org/10.1016/j.tsep.2018.03.011.
[43] Sardarabadi M, Hosseinzadeh M, Kazemian A, Passandideh-Fard M. Experimental investigation of the effects of using metal-oxides/water nanofluids on a photovoltaic thermal system (PVT) from energy and exergy viewpoints. Energy 2017;138:682–95. https://doi.org/10.1016/j.energy.2017.07.046.
[44] Park SR, Pandey AK, Tyagi VV, Tyagi SK. Energy and exergy analysis of typical renewable energy systems. Renew Sustain Energy Rev 2014;30:105–23. https://doi.org/10.1016/j.rser.2013.09.011.
[45] Said Z, Saidur R, Rahim NA, Alim MA. Analyses of exergy efficiency and pumping power for a conventional flat plate solar collector using SWCNTs based nanofluid. Energy Build 2014;78:1–9. https://doi.org/10.1016/j.enbuild.2014.03.061.
[46] Chow TT, Pei G, Fong KF, Lin Z, Chan ALS, Ji J. Energy and exergy analysis of photovoltaic–thermal collector with and without glass cover. Appl Energy 2009;86(3):310–6. https://doi.org/10.1016/j.apenergy.2008.04.016.
[47] Mahian O, Kianifar A, Sahin AZ, Wongwises S. Entropy generation during Al2O3/water nanofluid flow in a solar collector: Effects of tube roughness, nanoparticle size, and different thermophysical models. Int J Heat Mass Transf 2014;78:64–75. https://doi.org/10.1016/j.ijheatmasstransfer.2014.06.051.
[48] Azmi WH, Sharma KV, Sarma PK, Mamat R, Anuar S, Dharma Rao V. Experimental determination of turbulent forced convection heat transfer and friction factor with SiO2 nanofluid. Exp Therm Fluid Sci 2013;51:103–11. https://doi.org/10.1016/j.expthermflusci.2013.07.006.
[49] Zhang J, Diao YH, Zhao YH, Tang X, Yu WJ, Wang S. Experimental study on the heat recovery characteristics of a new-type flat micro-heat pipe array heat exchanger using nanofluid. Energy Convers Manag 2013;75:609–16. https://doi.org/10.1016/j.enconman.2013.08.003.
[50] Pounraj P, et al. Experimental investigation on Peltier based hybrid PV/T active solar still for enhancing the overall performance. Energy Convers Manag 2018;168:371–81. https://doi.org/10.1016/j.enconman.2018.05.011.
[51] Al-yasiri Q, Alshara A, Al-maliki I, Al-saadi H, Al-khafaji S. Effect of window-to-wall ratio and thermal insulation on building thermal energy in various Iraqi Cities. Misan J Eng Sci 2024;3(2):182–96. https://doi.org/10.61263/mjes.v3i2.117.
[52] Göksu TT. Enhancing cooling efficiency: innovative geometric designs and mono-hybrid nanofluid applications in heat sinks. Case Stud Therm Eng 2024;55(February):104096. https://doi.org/10.1016/j.csite.2024.104096.
[53] Allan J, Dehouche Z, Stankovic S, Mauricette L. Performance testing of thermal and photovoltaic thermal solar collectors. Energy Sci Eng 2015;3(4):310–26. https://doi.org/10.1002/ese3.75.
[54] Maatallah T, Zachariah R, Al-Amri FG. Exergo-economic analysis of a serpentine flow type water based photovoltaic thermal system with phase change material (PVT-PCM/water). Sol Energy 2019;193:195–204. https://doi.org/10.1016/j.solener.2019.09.063.
[55] Salem MR, Ali RK, Elshazly KM. Experimental investigation of the performance of a hybrid photovoltaic/thermal solar system using aluminium cooling plate with straight and helical channels. Sol Energy 2017;157:147–56. https://doi.org/10.1016/j.solener.2017.08.019.
[56] Poredoš P, Tomc U, Petelin N, Vidrih B, Flisar U, Kitanovski A. Numerical and experimental investigation of the energy and exergy performance of solar thermal, photovoltaic and photovoltaic-thermal modules based on roll-bond heat exchangers. Energy Convers Manag 2020;210:112674. https://doi.org/10.1016/j.enconman.2020.112674.